arXiv:1407.6285v1 [cond-mat.soft] 23 Jul 2014

Colloidal liquids of yolk-shell particles

L. E. Sanchez Diaz[†], E. C. Cortes-Morales[‡], X. Li[†],Wei-Ren Chen[†], and M. Medina-Noyola[‡]

[†]*Biology and Soft Matter Division, Oak Ridge National Laboratory, Oak Ridge, Tennessee 37831, USA and*

[‡]*Instituto de Física "Manuel Sandoval Vallarta", Universidad Autónoma de San Luis Potosí, Álvaro Obregón 64, 78000 San Luis Potosí, SLP, México*

(Dated: July 24, 2014)

Abstract

In this paper we develop statistical mechanical tools to describe the intermediate- and long-time collective- and self-diffusion properties of a liquid of strongly-interacting hollow spherical particles (shells), each bearing a smaller solid sphere (yolk) in its interior. To decouple two complex effects we assume that the hydrodynamic interactions can be accounted for through the effective short-time self-diffusion coefficients D_s^0 and D_y^0 that describe the short-time Brownian motion of the yolk and the shell particles, and develop a self-consistent generalized Langevin equation theory to describe the intermediate- and long-time effects of the direct shell-shell, yolk-shell and yolk-yolk interactions. In a concrete application, we consider the simplest yolk-shell model system involving purely repulsive hard-body interactions between all (shell and yolk) particles. Using a softened version of these interparticle potentials we perform Brownian dynamics simulations to determine the mean squared displacement of both types of particles, as well as the intermediate scattering function of the yolk-shell complex. We compare the theoretical and simulation results between them, and with the results for the same system in the absence of yolks. We find that the yolks, which have no effect on the shell-shell static structure, influences the dynamic properties in a predictable manner, fully captured by the theory.

PACS numbers: 64.70.Pf, 61.20.Gy, 47.57.J-

I. INTRODUCTION

The increased ability to manufacture colloidal particles with specific morphologies has presented colloid science with many new and fascinating challenges and opportunities. One example is provided by yolk-shell particles, i.e., hollow spherical particles (shells) bearing a smaller solid sphere (yolk) in its interior [1, 2]. Sophisticated nanostructures with this morphology can be synthesized for application in various fields such as biomedical imaging [3], catalysis [4], and energy storage devices [3]. Understanding the diffusive properties of individual yolk-shell particles when they operate in aqueous environments represents an interesting challenge. Manipulating their eventual self-assembly [5], or simply considering realistic conditions, requires a god understanding of the structure and dynamics of systems of interacting yolk-shell particles in terms of the yolk-yolk, yolk-shell, and shell-shell direct (i.e., conservative) and hydrodynamic interactions. It is not difficult to envision possible applications in many areas of materials design and engineering, of the condensed phases (liquids, crystals, and even glasses) that could be formed with yolk-shell particles.

One then would like to describe the effects of these interactions on, for example, the individual and the collective diffusive properties of yolk-shell particles immersed in a solvent at finite concentration. The dynamic properties of ordinary colloidal dispersion refer to the relaxation of the fluctuations $\delta n(\mathbf{r},t)$ of the local concentration $n(\mathbf{r},t)$ of colloidal particles around its bulk equilibrium value n. The average decay of $\delta n(\mathbf{r},t)$ is described by the time-dependent correlation function $F(k,t) \equiv \langle \delta n(\mathbf{k},t)\delta n(-\mathbf{k},0)\rangle$ of the Fourier transform $\delta n(\mathbf{k},t) \equiv (1/N)\sum_{i=1}^{N} \exp\left[i\mathbf{k}\cdot\mathbf{r}_i(t)\right]$ of the fluctuations $\delta n(\mathbf{r},t)$, with $\mathbf{r}_i(t)$ being the position of particle i at time t. $F(k,t)$ is referred to as the intermediate scattering function, measured by experimental techniques such as dynamic light scattering [6, 7]. One can also define the mean squared displacement $W(t) \equiv < (\Delta\mathbf{R}(t))^2 > /6$ and the self-intermediate scattering function, $F_S(k,t) \equiv \langle \exp\left[i\mathbf{k}\cdot\Delta\mathbf{R}(t)\right]\rangle$, where $\Delta\mathbf{R}(t)$ is the displacement of any of the N particles over a time t. The experimental and theoretical study of the dynamics of ordinary colloidal dispersion can be said to be fairly well established [6, 7]. One then would like to extend now the same level of understanding to yolk-shell suspensions. A basic and elementary question, for example, refers to the effect of the yolk-shell interaction on the Brownian motion of the complex, as exhibited by the difference between the Brownian motion of an empty shell, and of a shell carrying its yolk. A second question refers to the

effects of (direct and hydrodynamic) interactions between yolk-shells on the individual and collective diffusion of a concentarted suspension of strongly-interacting yolk-shell particles.

The detailed and simultaneous description of the coupled effects of direct and hydrodynamic interactions is, in general, a highly involved problem. We may profit, however, from the ingenious manners to decouple them, developed in similar challenges in colloid science [6, 7]. For example, at least for rigid shells, the complex effects of shell-shell hydrodynamic interactions can be taken into account through an effective self-diffusion coefficient D_s^0 describing the shells' short-time Brownian motion [8, 9]. Similarly, when focusing on the dynamics of condensed phases of strongly-interacting yolk-shell particles, the rich phenomenology of the hydrodynamic interactions of the captive yolk with its confining shell could also be modelled as a simple effective free-diffusion process, characterized by another effective (short-time) self-diffusion coefficient D_y^0, also amenable to independent experimental determination [10].

In an attempt to develop the simplest model representation of this class of materials, let us then assume that the hydrodynamic interactions can be accounted for through the effective short-time self-diffusion coefficients D_s^0 and D_y^0. In this context, the main purpose of the present work is to develop a statistical mechanical theory of the dependence of the collective- and self-diffusion properties of the yolk-shell suspensions, on control parameters such as the relative mobility of the shell and yolk particles (i.e., the ratio D_s^0/D_y^0), the specific geometry (size and thickness of the shell and size of the yolk), and the concentration of yolk-shell particles in the suspension. For this we develop a first-principles theory to predict the main features of the dynamic properties in terms of the specific effective interactions between the shell and the yolk particles that constitute the system. We approach this task in the framework of the self-consistent generalized Langevin equation (SCGLE) theory of colloid dynamics, which is adapted here to the context of a suspension of Brownian yolk-shell particles.

This paper is organized as follows. In Sec. II we define the model systems considered in our study and provide the basic information on the simulation methods employed. In Section III we adapt our self-consistent generalized Langevin equation (SCGLE) theory to the description of system of yolk-shell particles, and discuss very briefly the physical content and the rationale of each of the approximations involved in its formulation. In Sec IV we present and discuss the main results using Brownian dynamics simulations and compare

with the numerical solution of the full self-consistent theory. In Sec. V we develop the SCGLE theory of the yolk-shell systems in which yolk and shell particles are treated on the same footing. Finally, in Sec. VI we summarize our main conclusions.

II. MODEL SYSTEM AND BROWNIAN DYNAMICS SIMULATIONS

As our fundamental starting point, let us consider a model monodisperse yolk-shell colloidal suspension formed by N spherical shell particles in a volume V, each of which bears one smaller ("yolk") particle diffusing in its interior. Let us neglect hydrodynamic interactions and denote by $\mathbf{x}_i(t)$ and $\mathbf{v}_i(t)$ the position and velocity of the center of mass of the ith shell particle (with $i = 1, 2, \ldots, N$), and by $\mathbf{y}_i(t)$ and $\mathbf{w}_i(t)$ the position and velocity of the center of the ith yolk particle. The microscopic dynamics of these $2N$ Brownian particles is then described by the following $2N$ Langevin equations,

$$M_s \frac{d\mathbf{v}_i(t)}{dt} = -\zeta_s^0 \mathbf{v}_i(t) + \mathbf{f}_i^0(t) - \sum_{j\neq i} \nabla_i u_{ss}(|\mathbf{x}_i(t) - \mathbf{x}_j(t)|) - \sum_j \nabla_i u_{sy}(|\mathbf{x}_i(t) - \mathbf{y}_j(t)|), \quad (2.1)$$

$$M_y \frac{d\mathbf{w}_i(t)}{dt} = -\zeta_y^0 \mathbf{w}_i(t) + \mathbf{g}_i^0(t) - \sum_{j\neq i} \nabla_i u_{yy}(|\mathbf{y}_i(t) - \mathbf{y}_j(t)|) - \sum_j \nabla_i u_{ys}(|\mathbf{y}_i(t) - \mathbf{x}_j(t)|), \quad (2.2)$$

with $i = 1, 2, \ldots, N$. In these equations $\mathbf{f}_i^0(t)$ and $\mathbf{g}_i^0(t)$ are Gaussian white random forces of zero mean, and variance given by $\langle \mathbf{f}_i^0(t)\mathbf{g}_j^0(0)\rangle = 0$, $\langle \mathbf{f}_i^0(t)\mathbf{f}_j^0(0)\rangle = k_B T \zeta_s^0 2\delta(t)\delta_{ij} \overleftrightarrow{\mathbf{I}}$, and $\langle \mathbf{g}_i^0(t)\mathbf{g}_j^0(0)\rangle = k_B T \zeta_y^0 2\delta(t)\delta_{ij} \overleftrightarrow{\mathbf{I}}$, with $i, j = 1, 2, \ldots, N$ and with $\overleftrightarrow{\mathbf{I}}$ being the 3×3 unit tensor. The radially symmetric pairwise potentials $u_{ss}(r)$, $u_{sy}(r) = u_{ys}(r)$, and $u_{yy}(r)$ describe, respectively, the shell-shell, shell-yolk, and yolk-yolk direct interactions.

The microscopic dynamics represented by the $2N$ Langevin equations in Eqs. (2.5) and (2.6) constitute the starting point of both approaches employed to describe the self and collective dynamics of our system. Thus, the Brownian dynamics simulations below consist essentially of the numerical solution of these $2N$ stochastic Langevin equations. More precisely, according to the algorithm proposed by Ermak and McCammon [11], we solve the overdamped version of these equations, in which one neglects the inertial terms $M_s[d\mathbf{v}_i(t)/dt]$ and $M_s[d\mathbf{w}_i(t)/dt]$ on the left side of Eqs. (2.5) and (2.6). The resulting equations can be written as the following prescription to generate the new positions $\mathbf{x}_i(t+\Delta t)$ and $\mathbf{y}_i(t+\Delta t)$ from the current positions $\mathbf{x}_i(t)$ and $\mathbf{y}_i(t)$,

$$\mathbf{x}_i(t+\Delta t) = \mathbf{x}_i(t) + \beta D_s^0 \mathbf{F}_i(t)\Delta t + \mathbf{X}_i(t) \quad (2.3)$$

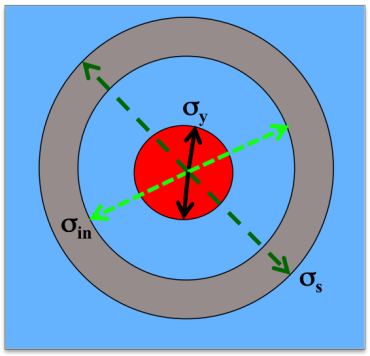

FIG. 1: A schematic representation of a yolk-shell particle. A mobile core of diameter σ_y is trapped inside a hollow spherical shell with inner diameter σ_{in} and outer σ_s.

and

$$\mathbf{y}_i(t+\Delta t) = \mathbf{y}_i(t) + \beta D_y^0 \mathbf{G}_i(t)\Delta t + \mathbf{Y}_i(t), \tag{2.4}$$

with $\beta^{-1} \equiv k_B T$ being the thermal energy and D_s^0 ($\equiv k_B T/\zeta_s^0$) and D_y^0 ($\equiv k_B T/\zeta_y^0$) being the short-time self-diffusion coefficients of the shell and yolk particles, respectively. In these equations $\mathbf{F}_i(t)$, defined as

$$\mathbf{F}_i(t) \equiv -\sum_{j\neq i} \nabla_i u_{ss}(|\mathbf{x}_i(t) - \mathbf{x}_j(t)|) - \sum_j \nabla_i u_{sy}(|\mathbf{x}_i(t) - \mathbf{y}_j(t)|), \tag{2.5}$$

is the force exerted by all the shells and yolks on the ith shell at time t, and $\mathbf{G}_i(t)$, defined as

$$\mathbf{G}_i(t) \equiv -\sum_{j\neq i} \nabla_i u_{yy}(|\mathbf{y}_i(t) - \mathbf{y}_j(t)|) - \sum_j \nabla_i u_{ys}(|\mathbf{y}_i(t) - \mathbf{x}_j(t)|), \tag{2.6}$$

is the force exerted by all the shells and yolks on the ith yolk. The random displacements $\mathbf{X}_i(t)$ ($\equiv +\beta D_s^0 \mathbf{f}_i^0(t)$) and $\mathbf{Y}_i(t)$ ($\equiv +\beta D_y^0 \mathbf{g}_i^0(t)$) are extracted from Gaussian distributions with zero mean and variance given, respectively, by $6D_s^0\Delta t$ and $6D_y^0\Delta t$.

In this work we apply this algorithm to the simplest model representation of a yolk-shell suspension, namely, a liquid of Brownian hollow spherical particles (shells), each bearing one smaller solid sphere (yolk), according to the schematic representation in Figure 1. The interactions between all (shell and yolk) particles will be represented by purely repulsive hard-body potentials. Thus, the shell-shell potential is

$$u_{ss}(r) = \begin{cases} \infty & \text{for } r < \sigma_s \\ 0 & \text{for } r > \sigma_s, \end{cases} \tag{2.7}$$

with σ_s being the outer diameter of the shells, the yolk-yolk interactions are non-existent, $u_{yy}(r) = 0$, and the yolk-shell interaction is defined by

$$u_{ys}(r) = \begin{cases} \infty & \text{for } r > \sigma_{ys} \equiv \frac{\sigma_{in}-\sigma_y}{2} \\ 0 & \text{for } r < \sigma_{ys}, \end{cases} \tag{2.8}$$

where σ_y is the diameter of the yolks and σ_{in} is the inner diameter of the shells.

The simulations were performed in a cubic simulation box. The minimum image convention and periodic boundary conditions were employed [12]. The initial configurations were generated using the following procedure. First, particles were placed randomly in the simulation box at the desired density and then the overlap between the particles are reduced or eliminated. Once the initial configuration is constructed, several thousand cycles are performed to lead the systems to equilibrium, followed by at least two million cycles where the data are collected. Throughout this paper we shall take σ_s and σ_s^2/D_s^0 as the units of length and time, respectively. In reality, the BD algorithm above is only defined for systems with continuous pair potentials. Thus, in practice we employ a softened version of the potential above to describe the interactions among yolk and shell particles. More specifically, we represent the hard-sphere interactions in Eqs. (2.7) and (2.8), by inverse power-law (IPL) potentials with amplitudes chosen such that, when written in units of k_BT, read

$$u_{ss}(r) = (\sigma_s/r)^{12} \tag{2.9}$$

or in the case of yolks, which only interact with their own shell, is given as

$$u_{ys}(r) = [\sigma_y/(\sigma_{ys} - r)]^{12} \tag{2.10}$$

where $\sigma_{ys} = (\sigma_{in} - \sigma_y)/2$ and σ_{in} is the inner diameter of the shell.

In order for the properties of this soft system to provide an accurate quantitative representation of the properties of the original hard system, one has to provide a precise prescription that assigns an equivalent soft system to any given hard system. Such prescription amounts to determine the inner shell diameter σ_{in}^{eff} of the effective soft system by the "blip function" condition, that the integral $\int \exp[-u_{ys}(r)]d^3r$ of the effective and the original hard systems coincide, and to determine the effective outer shell diameter σ_s^{eff} with the analogous blip function condition between the effective soft and the real hard shell-shell potentials. In practice, however, we actually employed a more precise determination of σ_s^{eff}, in which

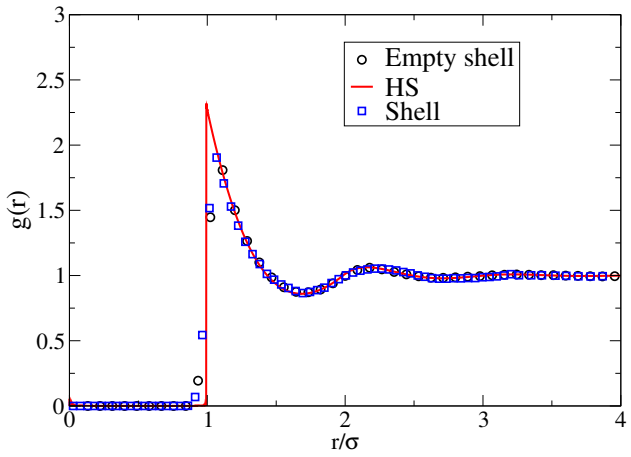

FIG. 2: Radial distribution function for shell-shell of the yolk-shell liquid (squares) and empty shell liquid (circles). Solid line corresponds to the Percus-Yevick approximation for HS with the Verlet-Weis correction a volume fraction $\phi = 0.3$.

(the second maximum of) the radial distribution function $g_{ss}(r)$ of the soft-sphere system coincides with that of the given HS system, as discussed in detail for solid spheres in Refs. [13, 14]. To illustrate this procedure, figure 2 plots the simulated $g_{ss}(r)$ of the soft system (symbols) with the $g_{ss}(r)$ corresponding to the hard system (solid line) at shell volume fraction $\phi = 0.3$. The latter is provided by the Percus-Yevick [15] approximation with its Verlet-Weis correction [16] (approximation denoted here as PYVW) for the liquid of hard spheres at volume fraction $\phi = 0.3$. The corresponding PYVW static structure factor $S(k)$ will also be employed as the structural input required by the SCGLE theory presented below. Having established the equivalence of hard and soft sphere systems, from now we will only refer to the shell volume fraction ϕ of the hard system.

The dynamic properties of the system above were then calculated from the equilibrium configurations generated by the BD simulations just described. Time correlation functions, like the mean-squared displacement (MSD) $W(t) =< [\Delta\vec{r}(t)]^2 > /6$ and the self-intermediate scattering function (self-ISF) $F_S(k,t)$ were calculated using the efficient, low-memory algorithm proposed in Ref. [17]. Later on in the paper these results will be discussed and employed to assess the numerical accuracy of the SCGLE theory for the yolk-shell systems developed in the following section.

III. SCGLE THEORY FOR YOLK-SHELL SUSPENSIONS.

In this section we outline the derivation of a first-principles statistical mechanical description of the dynamic properties of our model yolk-shell suspension. We approach this task in the framework of the self-consistent generalized Langevin equation (SCGLE) theory of colloid dynamics[18–23], which is thus adapted here to the context of a suspension of Brownian yolk-shell particles. The microscopic dynamics represented by the $2N$ Langevin equations in Eqs. (2.5) and (2.6), which was the basis for the derivation of the BD algorithm, also constitute the starting point of the present statistical mechanical derivations. In contrast with the strategy followed to derive the BD algorithm, in which we took the overdamped limit in these equations right at the outset, in the theoretical derivation below this limit is taken at a later stage. In fact, in the absence of the yolks, only the N Langevin equations in Eq. (2.5), with $u_{sy}(r) = 0$, remain, and these equations were taken as the starting point in the original derivation of the SCGLE theory for monodisperse suspensions. Thus, what we need now is to extend this derivation to the more general case in which we also have to deal with the presence of the yolks, i.e., with the terms involving the yolk-shell interactions $u_{sy}(r)$ and the additional N Langevin equations in Eq. (2.6). This task, however, follows essentially the same steps as the original derivation, and hence, here we only summarize the main arguments and the essential results, with some details being provided in the appendix.

Just like in the Brownian dynamics simulations, the present derivations will also be restricted to the case in which each yolk only interacts with its own shell. Under these conditions, Eqs. (2.5) and (2.6) simplify to

$$M_s \frac{d\mathbf{v}_i(t)}{dt} = -\zeta_s^0 \mathbf{v}_i(t) + \mathbf{f}_i^0(t) - \sum_{j\neq i} \nabla_i u_{ss}(|\mathbf{x}_i(t) - \mathbf{x}_j(t)|) - \nabla_{\mathbf{x}_i} u_{ys}(|\mathbf{x}_i(t) - \mathbf{y}_i(t)|) \quad (3.1)$$

and

$$M_y \frac{d\mathbf{w}_i(t)}{dt} = -\zeta_y^0 \mathbf{w}_i(t) + \mathbf{g}_i^0(t) - \nabla_{\mathbf{y}_i} u_{ys}(|\mathbf{y}_i(t) - \mathbf{x}_i(t)|). \quad (3.2)$$

This means that the motion of each yolk is only coupled with the motion of its own shell through the last term of these two equations (involving the pair potential $u_{ys}(|\mathbf{x}_i(t)-\mathbf{y}_i(t)|)$), while the motion of each shell is also coupled with the motion of all the other shells through the term involving the shell-shell pair potential $u_{ss}(|\mathbf{x}_i(t) - \mathbf{x}_j(t)|)$.

The general strategy that we shall adopt is to first average out the degrees of freedom (velocities and positions) of the yolk particles from the detailed description provided by Eqs.

(3.1) and (3.2) above, which involve the degrees of freedom of both, the shell and the yolk particles. This is equivalent to "solving" Eqs. (3.2) for the positions $\mathbf{y}_i(t)$ and velocities $\mathbf{w}_i(t)$ of the yolk particles, and substituting the solution in Eqs. (3.1). Such procedure, detailed in the appendix, yields the following set of N "renormalized" Langevin equations involving the positions and velocities of only the shell particles

$$M_s \frac{d\mathbf{v}_i(t)}{dt} = -\zeta_s^0 \mathbf{v}_i(t) - \int_0^t dt' \Delta\zeta_y(t-t')\mathbf{v}_i(t') + \mathbf{F}_i(t) - \sum_{j\neq i} \nabla_i u_{ss}(|\mathbf{x}_i(t) - \mathbf{x}_j(t)|) \quad (3.3)$$

for $i = 1, 2, \ldots, N$, where the random force $\mathbf{F}_i(t)$ has zero mean and correlation function given by $\langle \mathbf{F}_i(t)\mathbf{F}_j(0)\rangle = k_B T[\zeta_s^0 2\delta(t) + \Delta\zeta_y(t)]\delta_{ij} \overleftrightarrow{\mathbf{I}}$ (with $i, j = 1, 2, \ldots, N$), with the time-dependent friction function $\Delta\zeta_y(t)$ given by the *approximate* result in Eq. (A12), namely,

$$\Delta\zeta_y(t) = \frac{k_B T n_0}{3(2\pi)^3} \int d^3k [k g_{ys}(k)]^2 e^{-k^2 D_y^0 t} F_S(k,t). \quad (3.4)$$

In this equation $F_S(k,t)$ is the self intermediate scattering function of the shell particles and $g_{ys}(k)$ is the Fourier transform of $g_{ys}(r) \equiv \exp[-\beta u_{ys}(r)]$, i.e., $n_0 g_{ys}(r)$ is the probability distribution function that the center of the yolk lies a distance r apart from the center of the shell, normalized such that $n_0 \equiv 1/\int \exp[-\beta u_{ys}(r)] d^3r$.

The second stage in this strategy is to take the set of N "renormalized" Langevin equations in Eq. (A11) as the starting point of the derivation of three results that are central to the formulation of the SCGLE theory. The first is a generalized Langevin equation for a single tracer shell particle, which effectively takes into account its interactions with the rest of the "renormalized" shells. This amounts to solving $(N-1)$ of the Langevin equations in Eq. (A11) (for, say, $i = 2, ..., N$), and to use the result in Eq. (A11) for $i = 1$. This leads to the desired generalized Langevin equation which, with the label $i = 1$ changed to "T" (for "tracer"), reads

$$M_s \frac{d\mathbf{v}_T(t)}{dt} = -\zeta_s^0 \mathbf{v}_T(t) - \int_0^t dt' \Delta\zeta_y(t-t')\mathbf{v}_T(t') - \int_0^t dt' \Delta\zeta_s(t-t')\mathbf{v}_T(t') + \mathbf{F}(t). \quad (3.5)$$

The random force $\mathbf{F}(t)$ in this equation has zero mean and correlation function given now by $\langle \mathbf{F}(t)\mathbf{F}(0)\rangle = k_B T[\zeta_s^0 2\delta(t) + \Delta\zeta_y(t) + \Delta\zeta_s(t)] \overleftrightarrow{\mathbf{I}}$, with the new time-dependent friction function $\Delta\zeta_s(t)$ representing the friction on the tracer shell particle due to its direct interactions with the other shells.

Except for the presence of the additive yolk friction term $-\int_0^t dt' \Delta\zeta_y(t-t')\mathbf{v}_T(t')$, the derivation of this equation follows step by step the derivation originally carried out for

Brownian liquids of "compact" (not yolk-shell) particles [24]. Thus, here we omit the details of such derivation, which leads to an exact expression for $\Delta\zeta_s(t)$. As argued in that reference, after a set of well-defined approximations, also adopted in the present case, such an exact expression becomes

$$\Delta\zeta_s(t) = \frac{k_B T}{3\,(2\pi)^3\, n} \int d\mathbf{k} \left[\frac{k[S(k)-1]}{S(k)}\right]^2 F(k,t) F_S(k,t), \tag{3.6}$$

where $S(k)$ is the (shell-shell) static structure factor, and $F(k,t)$ and $F_S(k,t)$ are the collective and the self intermediate scattering functions.

In order to evaluate $\Delta\zeta_y(t)$ and $\Delta\zeta_s(t)$ we thus need to determine $F(k,t)$ and $F_S(k,t)$. This task involves the derivation of the other two general results, namely, the (exact) memory function expressions for $F(k,t)$ and $F_S(k,t)$, starting again from the mesoscopic description provided by the set of N "renormalized" Langevin equations in Eq. (A11). Here too, except for the presence of the additive yolk friction terms in the right side of these equations, such derivation follows step by step the corresponding derivation for "solid" particles described in Ref. [18], and hence, we also omit the details. Furthermore, in the present case we adopt the same set of approximations summarized in Ref. [23] to turn those exact memory function expressions into useful approximate results (adapted here to include the presence of the yolk friction function $\Delta\zeta_y(t)$). These are the Vineyard-like approximation, in which one approximates the memory function $C(k,t)$ of the collective ISF $F(k,t)$ by the memory function $C_S(k,t)$ of the *self* ISF $F_S(k,t)$, along with the approximation that writes $C_S(k,t)$ as the superposition of the normalized (yolk) friction function $\Delta\zeta_y^*(t) \equiv \Delta\zeta_y(t)/\zeta_s^0$ plus the contribution due to shell-shell interactions, factorized as the product of its long wave-length limit $\Delta\zeta_s^*(t) \equiv \Delta\zeta_s(t)/\zeta_s^0$ times a phenomenological "interpolating function" $\lambda(k)$. This results in the following approximate expressions for $F(k,z)$ and $F_S(k,z)$,

$$F(k,z) = \frac{S(k)}{z + \frac{k^2 S^{-1}(k) D_s^0}{1+\Delta\zeta_y^*(z)+\lambda(k)\Delta\zeta_s^*(z)}} \tag{3.7}$$

and

$$F_S(k,z) = \frac{1}{z + \frac{k^2 D_s^0}{1+\Delta\zeta_y^*(z)+\lambda(k)\Delta\zeta_s^*(z)}}, \tag{3.8}$$

where $\lambda(k)$ is given by [23]

$$\lambda_\alpha(k) = 1/[1+(k/k_c)]^2, \tag{3.9}$$

and k_c is an empirical cutoff wave-vector. In this paper we shall use the value $k_c = 1.305(2\pi/\sigma)$, which results from a previous calibration [25] of the SCGLE theory with simulation data for the hard-sphere system, a limit that we must recover in the absence of yolks, i.e., when $\Delta\zeta_y^*(z) = 0$.

Eqs. (3.4) and (3.6)-(3.9) above constitute the extension of the SCGLE description of the dynamics of a liquid of yolk-shell particles. The simultaneous solution of these equations for given static structural properties $g_{ys}(k)$ and $S(k)$ determines the time-dependent friction functions $\Delta\zeta_y^*(t)$ and $\Delta\zeta_s^*(z)$ and the intermediate scattering functions $F(k,t;\phi)$ and $F^S(k,t;\phi)$. The mean squared displacement $W(t;\phi)$ then derives from $\Delta\zeta_y^*(t)$ and $\Delta\zeta_s^*(t;\phi)$ according to

$$W(t;\phi) = D_s^0 t - \int_0^t \left[\Delta\zeta_y^*(t-t') + \Delta\zeta_s^*(t-t';\phi)\right] W(t';\phi)dt'. \tag{3.10}$$

The solution of Eqs. (3.4) and (3.6)-(3.10) for the yolk-shell model system described in the previous section will now be discussed.

IV. RESULTS

In this section we present our theoretical and simulated results for the properties that describe the Brownian motion of a tagged yolk-shell complex. Our intention is to describe how the mean squared displacement and the self intermediate scattering function of such tagged yolk-shell particles are influenced by the combined effect of the interaction of the shell with its own yolk and with the other shells as we vary the concentration $n \equiv N/V$ of yolk-shell particles, actually indicated in terms of the shell volume fraction $\phi \equiv \pi n \sigma_s^3/6$. To simplify the discussion, we shall begin with the description of the properties of a single yolk-shell complex, which diffuses without interacting with other yolk-shell particles, i.e., with the $\phi \to \infty$ limit. Under these conditions, the shell-shell friction function $\Delta\zeta_s^*(t;\phi)$ vanishes and one only has to solve simultaneously Eqs. (3.4) and (3.8) for $\Delta\zeta_s^*(t)$ and $F^S(k,t;\phi)$.

After discussing this infinite dilution limit, we shall study the additional effects that derive from the shell-shell interactions at given finite concentrations of yolk-shell complexes. One important aspect of our discussion in both concentration regimes, however, will refer to the comparison of these properties with those of a system of empty shells (i.e., of the same system but in the absence of the yolk particles). This simpler system is actually identical to

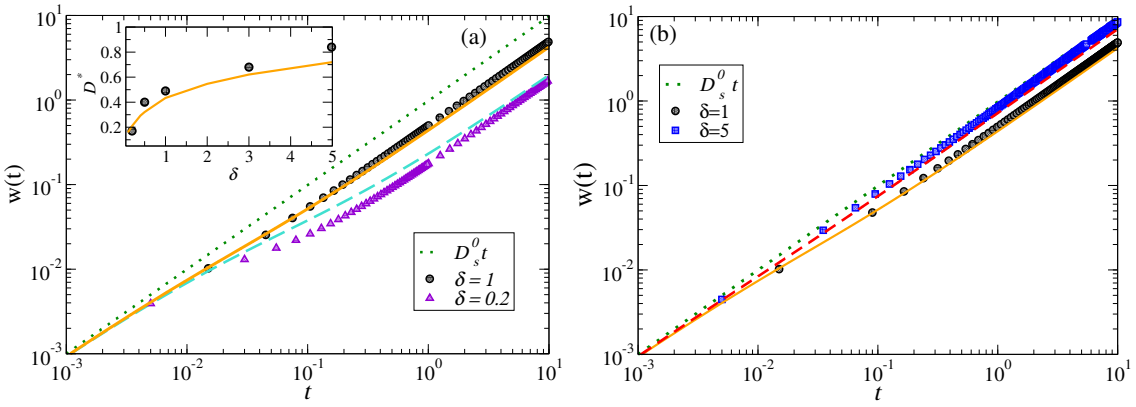

FIG. 3: Mean square displacement $W(t;\phi=0)$ of non-interacting yolk-shell particles with shell thickness $(\sigma_s-\sigma_{in})/2 = 0.05$ (or $\sigma_{in}=0.9$) and yolk diameter $\sigma_y = 0.2$. We recall that we are taking σ_s as the units of length and σ_s^2/D_s^0 as the time unit. The dotted line represents the MSD $W_0(t;\phi=0) = D_s^0 t$ of a freely diffusing empty shell. The circles are the Brownian dynamics data and the solid line is the theoretical prediction of the SCGLE theory corresponding to a dynamic asymmetry parameter $\delta \equiv D_y^0/D_s^0 = 1$. The squares and the dashed line in (a) correspond to $\delta = 0.2$, and the triangles and dot-dashed line in (b) correspond to $\delta = 5$. Finally the inset in figure (a) we compare the simulation and theoretical results for the long-time self-diffusion D^* as function δ.

an ordinary suspension of hard-sphere particles without hydrodynamic interactions, whose properties will be denoted as $W_0(t;\phi)$ and $F_0^S(k,t;\phi)$. Theoretically, these properties are obtained from the solution of Eqs. (3.6)-(3.10) with $\Delta\zeta_y^*(t) = 0$.

Finally, in the last section, we discuss the extension of the SCGLE theory to consider other, more complex conditions. Here we consider the case when the interaction between shells were to be attractive rather than repulsive, but in which the interaction of the yolk-shell otherwise remains the same. We then also compare the results of yolk-shell complex with a system of empty shells as function of temperature.

A. Yolk-shell self-diffusion in the dilute limit

Let us thus start by analyzing the results of our Brownian Dynamics simulations for the mean squared displacement $W(t;\phi=0)$ of a freely-diffusing yolk-shell complex, which we present in Fig 3 (symbols). Let us mention that all the results discussed in this figure,

and in general in the present section, correspond to a fixed yolk-shell geometry, in which the thickness $(\sigma_s - \sigma_{in})$ of the shell is 5% the shell's outer diameter, $\sigma_{in}/\sigma_s = 0.9$, and the yolk's diameter is 0.2 in units of σ_s, i.e., $\sigma_y/\sigma_s = 0.2$. The three different symbols in Fig 3 correspond to three different values of the ratio $\delta \equiv D_y^0/D_s^0$, which measures the dynamic asymmetry in the short-time diffusion of the yolk and the shell particles. These values are $\delta = 0.2,\ 1$, and 5. Let us first focus only on the circles, corresponding to the BD simulation results for $\delta = 1$, and on the dotted line representing the MSD $W_0(t;\phi = 0) = D_s^0 t$ of a freely diffusing empty shell. The deviation of the simulation data from $W_0(t;\phi = 0)$ is a measure of the additional friction effects on the displacement of the complex due to the yolk-shell interaction. The solid line that follows the BD data in circles are the prediction of our SCGLE theory obtained, as indicated above, by simultaneously solving Eqs. (3.4) and (3.8) for $\Delta\zeta_s^*(t)$ and $F^S(k,t;\phi)$, and then solving Eq. (3.10) with $\Delta\zeta_s^*(t;\phi = 0) = 0$ to obtain $W(t;\phi = 0)$. The first conclusion that we can draw from this comparison is that the SCGLE-predicted deviation of $W(t;\phi = 0)$ from $W_0(t;\phi = 0)$, coincides very satisfactorily with the deviation observed in the BD data.

The next conclusion to draw from the results in Fig. 3(a) is that the deviation of $W(t;\phi = 0)$ from $W_0(t;\phi = 0)$ increases when the dynamic contrast parameter δ decreases. This is illustrated by the comparison of the BD simulations corresponding to $\delta = 0.2$ (squares) with the BD data corresponding to $\delta = 1.0$ (circles). This means, for example, that if the interior of the shell becomes more viscous, so that the ratio δ decreases, then also the overall diffusivity of the yolk-shell particle will decrease. As evidenced by the solid and dashed lines in Fig. 3(a), this trend is also predicted by the SCGLE theory, in good quantitative agreement with the simulation data. In fact, our theory predicts, and the simulations corroborate, that this trend is reversed when one considers the opposite limit, in which δ is now larger than 1, as illustrated in Fig. 3(b), where we compare the (theoretical and simulation) results corresponding to $\delta = 5$ (triangles and dashed line) with the previous results for $\delta = 1$ (circles and solid line).

As illustrated by the results in Fig. 3, the MSD of the yolk-shell complexes exhibits two linear regimes. At short times $W(t) \approx D_s^0 t$ and at long times $W(t) \approx D_L t$, where D_L is the long-time self-diffusion coefficient. Thus, D_L, normalized as $D^*(\phi) \equiv D_L/D_s$, is obtained from the long-time slope of the msd, i.e, $D^*(\phi) = \lim_{t\to\infty} < W(t) > /D_s^0 t$. The results for $D^*(\phi = 0)$, obtained from the predicted and simulated results for $W(t;\phi = 0)$ in this figure

corresponding to different values of the dynamic asymmetry parameter δ, are summarized in the inset of Fig. 3(a), which plots $D^*(\phi = 0)$ as a function of δ. There we can see that the reduction of the mobility $D^*(\phi = 0)$ from its unit value in the absence of yolks, may be considerable. For example, for $\delta = 0.2$ we have that $D^* \approx 0.17$. A reduction of $D^*(\phi)$ of a similar magnitude in a system in which yolk-shell interactions have been suppressed (i.e., in the absence of yolks) can also be produced as a result of pure shell-shell interactions, but only at shell volume fractions above 40%. This can be concluded from the results of the inset in Fig. 5b of the following section, which discusses the effects of shell-shell interactions.

An additional important factor for the yolk-shell diffusion could be the effect of the geometry of the particle. For example, the effect of the size of the yolk. Fig. 4 shows the mean square displacement when we increase the size of the yolk, measured using the ratio $\delta_\sigma \equiv \sigma_y/2\sigma_{ys}$ with fixed inner diameter $\sigma_{in} = 0.9$ and $\delta \equiv D_y^0/D_s^0 = 1$. Circles correspond to the previous results shown in figure 3, in which the size of the yolk was $\sigma_y = 0.2$ ($\delta_\sigma = 0.28$) with $\delta \equiv D_y^0/D_s^0 = 1$. Also the dotted line represents the MSD $W_0(t;\phi = 0) = D_s^0 t$ of a freely diffusing empty shell. If we increase the size of the yolk until the inner space is filled 80%, i.e. $\delta_\sigma = 0.8$, we notice the deviation between $W(t;\phi = 0)$ and $W_0(t;\phi = 0)$ begins to more closely resemble the diffusion of the empty shell. This is illustrated by the comparison of the BD simulations corresponding to $\delta_\sigma = 0.8$ (triangles) with the BD data corresponding to $\delta_\sigma = 0.28$ (circles). This suggests that, when the size of the yolk increases, the yolk has less space for diffusion, and the additional friction effects upon the displacement of the complex due to the yolk-shell interaction decrease. The effect is similar to that found when the inside the yolk diffuses in medium less viscous than the shell. As evidenced by the solid and dotted lines in Fig. 4, this trend is also predicted by the SCGLE theory, showing good quantitative agreement with the simulation data. Finally the inset of Fig. 4 plots $D^*(\phi = 0)$ as a function of δ_σ. There we can see the reduction of the mobility $D^*(\phi = 0)$ when we decrease the size of the yolk. For example, for $\delta_\sigma = 0.5$, we have that $D^* \approx 0.65$.

B. Yolk-shell diffusion at finite concentration

Let us now study the effects of shell-shell interactions on the Brownian motion of tagged yolk-shell particles, which for simplicity were suppressed in the previous discussion. These effects manifest themselves only at finite concentrations. Thus, let us begin by analyzing

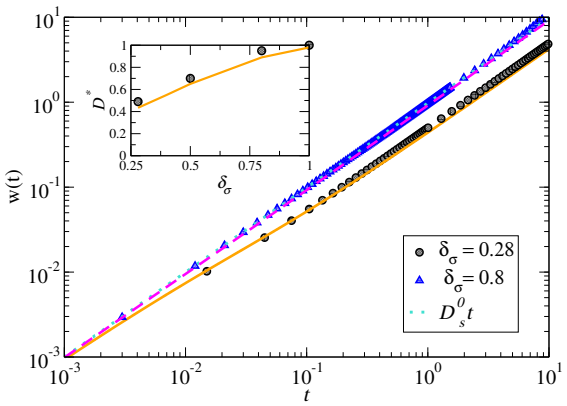

FIG. 4: Mean square displacement $W(t;\phi=0)$ of non-interacting yolk-shell particles with shell thickness $(\sigma_s-\sigma_{in})/2 = 0.05$ (or $\sigma_{in} = 0.9$) as a function of the $\delta_\sigma \equiv \sigma_y/2\sigma_{ys}$. We recall that we are taking σ_s as the units of length and σ_s^2/D_s^0 as the time unit. The dotted line represents the MSD $W_0(t;\phi=0) = D_s^0 t$ of a freely diffusing empty shell. The circles are the Brownian dynamics data and the solid line is the theoretical prediction of the SCGLE theory corresponding to a $\delta_\sigma = 0.28$. The triangles and the dashed line correspond to $\delta_\sigma = 0.8$. Finally the inset in figure we compare the simulation and theoretical results for the long-time self-diffusion D^* as function δ_σ.

the results of our simulations in Fig. 5a, where the circles represent the BD results for the MSD $W(t;\phi=0.15)$ of yolk-shell particles with dynamic asymmetry $\delta = 1$ at a finite but low volume fraction $\phi = 0.15$. These results are to be compared with the squares, which correspond to the BD results for the MSD $W_0(t;\phi=0.15)$ of a liquid of empty shells (or solid hard-spheres) at the same volume fraction $\phi = 0.15$, and which diffuse with the same short-time self-diffusion coefficient D_s^0 as the shells in the yolk-shell system. The MSD $W_0(t;\phi=0) = D_s^0 t$ of a freely diffusing empty shell is also plotted for reference as a dotted line. Clearly, at this low volume fraction the MSD $W_0(t;\phi=0.15)$ of the hard-sphere liquid is very similar to $W_0(t;\phi=0) = D_s^0 t$. In contrast, the yolk-shell interactions present in the yolk-shell system leads to a MSD $W(t;\phi=0.15)$ that clearly deviates from the empty shell result.

Upon increasing the volume fraction to $\phi = 0.4$ (Fig. 5b), we observe that the deviation of $W(t;\phi=0.4)$ from $W_0(t;\phi=0.4)$ remains rather similar to the corresponding deviation observed at $\phi = 0.15$ in Fig. 5a. We also observe that both, $W(t;\phi=0.4)$ and $W_0(t;\phi=0.4)$, now deviate dramatically from the free-diffusion limit $W_0(t;\phi=0) = D_s^0 t$. This means that for this concentration the mutual friction effects due to shell-shell interactions

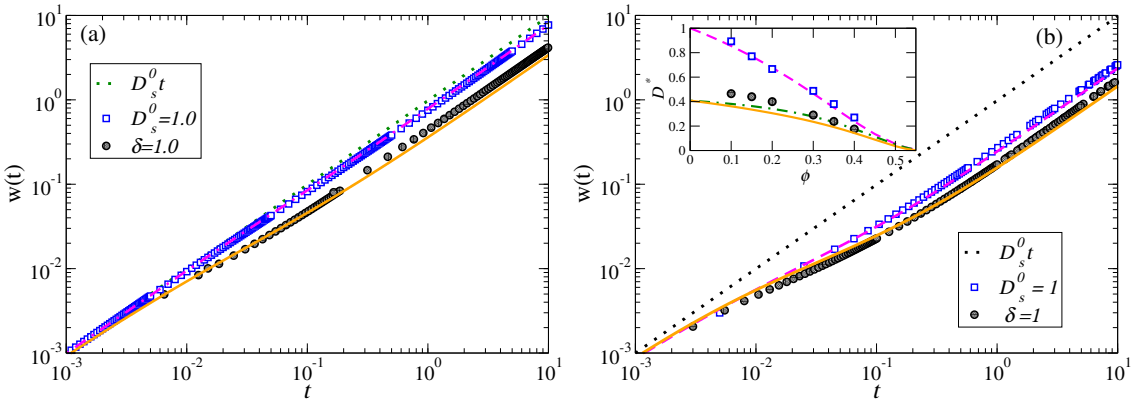

FIG. 5: Mean square displacement $W(t;\phi = 0.15)$ (a) and $W(t;\phi = 0.4)$ (b) of interacting yolk-shell particles with shell thickness $(\sigma_s - \sigma_{in})/2 = 0.05$ (or $\sigma_{in} = 0.9$) and yolk diameter $\sigma_y = 0.2$. We recall that we are taking σ_s as the units of length and σ_s^2/D_s^0 as the time unit. The dotted line represents the MSD $W_0(t;\phi = 0) = D_s^0 t$ of a freely diffusing empty-shell. The circles are the Brownian dynamics data for the yolk-shell and the solid line is the theoretical prediction of the SCGLE theory corresponding to a dynamic asymmetry parameter $\delta = 1$. The squares are the Brownian dynamics data of the empty-shell and the dashed line is the theoretical prediction of the SCGLE theory with $D_s^0 = 1$. Finally the inset in figure (b) we compare the simulation data and theoretical results for the long-time self-diffusion D^* as function ϕ.

overwhelm the "internal" friction effects due to yolk-shell interactions. From the long-time BD data for $W(t;\phi = 0.4)$ and $W_0(t;\phi = 0.4)$ in Fig. 5b we can extract the value of $D^*(\phi)$ and $D^*_{HS}(\phi)$, which represent the mobility of a tracer yolk-shell particle and of an empty shell, respectively. The results are plotted in the inset of this figure, together with the corresponding BD results for $D^*(\phi)$ and $D^*_{HS}(\phi)$ at other volume fractions (circles and squares, respectively). This inset thus summarizes the main trends illustrated by the results in Fig. 5, by evidencing that at low volume fractions the difference between the mobility of a yolk-shell complex and the mobility of an empty shell, is determined only by the yolk-shell friction, whereas at higher concentrations it is dominated by the shell-shell interactions.

Let us notice now that the solid lines in Fig. 5 represent again the predictions of the SCGLE theory for the properties of the yolk-shell system, whereas the dashed lines are the corresponding predictions for the empty-shell (or hard-sphere) suspension. Once again, the agreement with the simulation results is also quite reasonable for a theory with no adjustable parameters. Beyond this quantitative observation, however, the theoretical description pro-

vides additional insights on the interpretation of the qualitative trends exhibited by the simulation data of the long-time self-diffusion coefficients $D^*(\phi)$ and $D^*_{HS}(\phi)$. To see this, let us define $\Delta\zeta^*_y \equiv \int_0^\infty dt \Delta\zeta^*_y(t)$ and $\Delta\zeta^*_s(\phi) \equiv \int_0^\infty dt \Delta\zeta^*_s(t;\phi)$, and let us write Einstein's relation for D_L as

$$D^*(\phi) = \frac{1}{1 + \Delta\zeta^*_y + \Delta\zeta^*_s(\phi)}, \tag{4.1}$$

or, in terms of the low-density limit $D^*_0 \equiv D^*(\phi = 0) = [1 + \Delta\zeta^*_y]^{-1}$, as

$$D^*(\phi) = \frac{D^*_0}{1 + D^*_0 \Delta\zeta^*_s}. \tag{4.2}$$

Since for an empty shell (or hard-sphere) $\Delta\zeta^*_y = 0$, so that $D^*_0 = 1$, we have that the empty-shell version of this equation is

$$D^*_{HS}(\phi) = \frac{1}{1 + \Delta\zeta^{*HS}_s(\phi)}. \tag{4.3}$$

Thus, if we now assume that the shell-shell friction on a yolk-shell particle is comparable to the friction $\Delta\zeta^{*HS}_s$ in an empty-shell suspension, we may combine Eqs. (4.2) and (4.3) to write an approximate relationship between $D^*(\phi)$ and $D^*_{HS}(\phi)$, namely,

$$D^*(\phi) = \frac{D^*_0 \times D^*_{HS}(\phi)}{D^*_{HS}(\phi) + D^*_0[1 - D^*_{HS}(\phi)]}. \tag{4.4}$$

This expression interpolates $D^*(\phi)$ between its exact low and high concentration limits D^*_0 and $D^*_{HS}(\phi)$, and the dot-dashed line in the inset of Fig. 5 is the result of using this approximate expression.

We next analyze the results for the self-intermediate scattering function of shell-shell $F^s(k,t)$ obtained of our simulation. Let us first discuss the results in figure 6a, where the circles represent the BD results for the self-ISF $F^s(k,t;\phi = 0.15)$ of yolk-shell particles with dynamic asymmetry $\delta = 1$ at a volume fraction $\phi = 0.15$. We compare these results with the self-ISF $F^s_0(k,t;\phi = 0.15)$ of a liquid of empty-shells at the same volume fraction and with short-time self-diffusion coefficient $D^0_s = 1$, plotted as squares. The self-ISF $F^s_0(k,t;\phi = 0) = exp(-k^2 D^0_s t)$ of a freely diffusing empty shell is also plotted for reference as a dotted line. We evaluate the self-ISF for three cases at $k = 6.18$, which is approximately the first peak of the $S(k)$. The relaxation of the empty shell $F^s_0(k,t;\phi = 0.15)$ shows a single, exponential-like decay similar to $F^s_0(k,t;\phi = 0)$. We observe that the relaxation of $F^s(k,t;\phi = 0.15)$ suffers a deviation from $F^s_0(k,t;\phi = 0.15)$, and this is also evidence of the additional friction effect upon the yolk-shell interaction.

Upon increasing the volume fraction to $\phi = 0.4$ (Fig. 6b), we observe that the deviation of $F^s(k,t;\phi=0.4)$ from $F_0^s(k,t;\phi=0.4)$ remains rather similar to the corresponding deviation observed at $\phi = 0.15$ in Fig. 5a. We also observe that both, $F^s(k,t;\phi=0.4)$ and $F_0^s(k,t;\phi=0.4)$ now deviate dramatically from the free-diffusion limit $F_0^s(k,t;\phi=0)$. This further corroborates with the observations of the MSD. The theoretical predictions for the liquid of yolk shell (solid line) follow with good agreement the simulation data for $\phi = 0.15$ and show slight deviation for $\phi = 0.4$. The empty-shell (dashed line) also shows good agreement.

The difference between the yolk-shell and empty-shell results can also be expressed more economically in terms of the corresponding α-relaxation times τ_α, defined by the condition $F_S(k,\tau_\alpha) = 1/e$ and scaled as $\tau^* \equiv k^2 D_s^0 \tau_\alpha$. The inset of Fig. 6b exhibits the theoretical (solid line) and simulated (circles) results for the yolk-shell $\tau^*(k;\phi,\delta)$ evaluated at $k = 6.18$ for $\delta = 1$ as a function of ϕ. These results may be compared with the theoretical (dashed line) and simulated (squares) results for $\tau^*_{HS}(k = 6.18;\phi = 0.4)$, corresponding to the empty-shell suspension, with similar conclusions as in Fig. 5b. In analogy with the relationship in Eq. (4.4), from the SCGLE equations one can also derive an approximate relationship between $\tau^*(k;\phi,\delta)$ and $\tau^*_{HS}(k;\phi)$, namely, $\tau^*(k;\phi,\delta) \approx \tau^*_{HS}(k;\phi) + \Delta\zeta^*_y(\delta)$. This prediction of the value of $\tau^*(k;\phi,\delta)$ has a rather modest quantitative accuracy, as indicated by the dot-dashed line in the inset. Still, it contributes to a simple and correct qualitative understanding of the main features of the properties of the yolk-shell system being studied.

The previous results demonstrated the SCGLE theory to predict, with good agreement, the different results obtained with BD simulations of the yolk-shell complex. Based upon this agreement, our theoretical approach may be extended to consider other, more complex conditions. For example, the previous results only showed BD simulation data to below a volume fraction of $\phi = 0.5$. But here, we also demonstrate the use of the theory to calculate dynamic properties of the yolk-shell at high volume fractions. This is shown in figure 7, which plots the inverse of the long time self-diffusion coefficient $1/D^*$ and *α-relaxation* time $\tau^* \equiv k^2 D_s^0 \tau_\alpha$ as a function of the volume fraction ϕ beyond $\phi = 0.5$. The solid curve shows the theoretical prediction for the yolk-shell complex with $\delta = 1$. The dashed line represents the theoretical prediction for the empty shell with $D_s^0 = 1$. For both figures we note that, upon increasing the volume fraction, the difference between the yolk-shell and empty shell diffusion progressively decreases. Beyond $\phi = 0.56$, both systems appear to demonstrate the same dynamic behavior. This suggests that the shell-shell interaction is

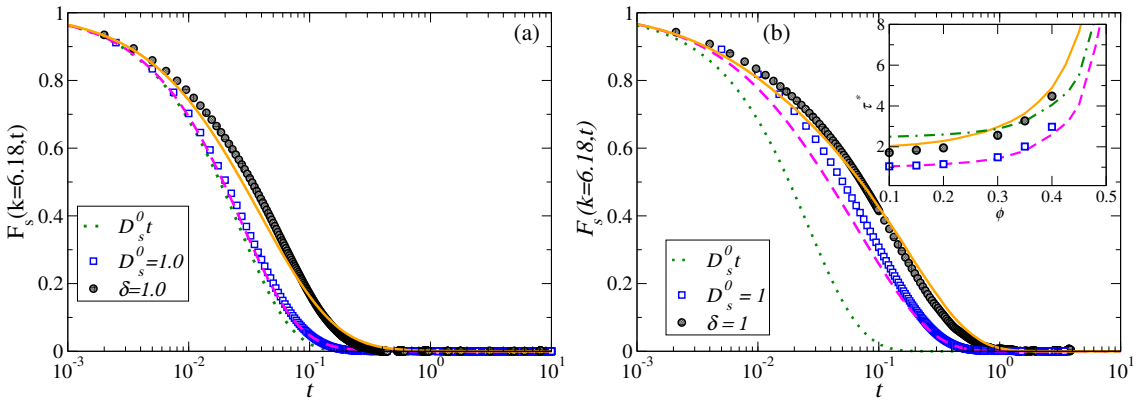

FIG. 6: The self-intermediate $F^s(k,t;\phi=0.15)$ (a) and $F^s(k,t;\phi=0.4)$ (b) of interacting yolk-shell particles with shell thickness $(\sigma_s-\sigma_{in})/2=0.05$ (or $\sigma_{in}=0.9$) and yolk diameter $\sigma_y=0.2$. We recall that we are taking σ_s as the units of length and σ_s^2/D_s^0 as the time unit. The dotted line represents the self-ISF $F_0^s(k,t;\phi=0)=exp(-k^2D_s^0t)$ of a freely diffusing empty shell. The circles are the Brownian dynamics data for the yolk-shell and the solid line is the theoretical prediction of the SCGLE theory with $\delta=1$. The squares are the Brownian dynamics data of the empty-shell and the dashed line is the theoretical prediction of the SCGLE theory with $D_s^0=1$. Finally the inset in figure (b) we compare the simulation data and theoretical results for the α-relaxation time $\tau^*\equiv k^2D_s^0\tau_\alpha$ as function ϕ.

more dominant than the yolk-shell interaction. We observe that at approximately $\phi=0.58$, both systems appear to show a clear divergence, indicating the dynamic arrest transition as predicted for a hard-sphere system (previously predicted SCGLE theory in the ref[23]) . We can conclude that the additional friction effect upon the displacement of the complex due to the yolk-shell interaction is not important when approaching the glass transition of hard spheres.

C. Effects of shell-shell attractions

Another possible application of the SCGLE theory is to consider the possibility that the interaction between shells include an attractive component, besides the hard-core repulsive interaction just described. Such interaction between shells could be described adding a simple 'attractive Yukawa' term to the hard-sphere potential $u_{ss}(r)$ in Eq. (2.7), which now

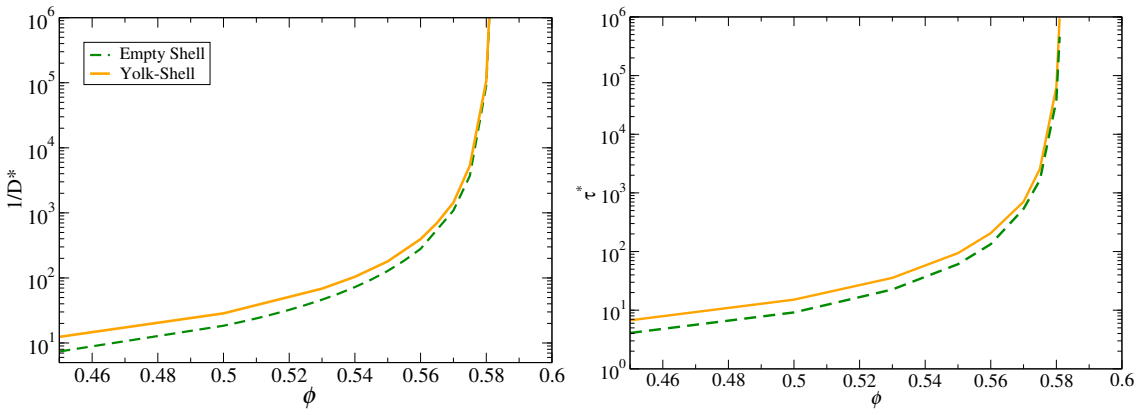

FIG. 7: The long time self-diffusion coefficient D^* and α-*relaxation* time $\tau^* \equiv k^2 D_s^0 \tau_\alpha$as function of the volume fraction ϕ. The solid line is theoretical results for the yolk-shell complex. The dashed line is theoretical results of the empty shell.

would be given by

$$\beta u_{ss}(r) = \begin{cases} \infty & \text{for } r < \sigma_s \\ -K \frac{exp[-z(r/\sigma_s - 1))]}{r/\sigma_s} & \text{for } r > \sigma_s, \end{cases} \tag{4.5}$$

An ordinary suspension with attractive interactions exhibits interesting phase behavior and structural and dynamic properties [26, 27]. Our yolk-shell system, in which the yolk-shell interactions remains the same as that of the equation (2.8), also exhibits similar behavior. The state space of this system is spanned by the hard-sphere volume fraction of the shell and by dimensionless parameters z and K, representing the inverse decay length and the depth of the attractive Yukawa well. For the calculation of the static structure factor for the shell, we can use the mean spherical approximation (MSA) described in reference [28].

Let us now study the effects of shell-shell interactions on the Brownian motion of tagged yolk-shell particles. For this case, we want to see if the effect of attraction is influencing the dynamics of the yolk-shell complex, and compare this with the dynamics of the empty shell, also with attractive interaction. We fixed the system with $z = 20$ and $\phi = 0.35$, and lowered temperatures for three different temperatures $T^* = 0.5$, 0.065 and 0.052. In figure 8, we show the prediction of the SCGLE theory of the mean square displacement and self-intermediate scattering function as a function of temperature $T^* = (1/K)$. Let us begin by analyzing the results in Fig. 8a, where the solid lines represent the prediction of SCGLE theory results for the MSD $W(t; T^* = 0.5)$ of yolk-shell particles with dynamic asymmetry $\delta = 1$ at a temperature $T^* = 0.5$. These results are to be compared with the dash line,

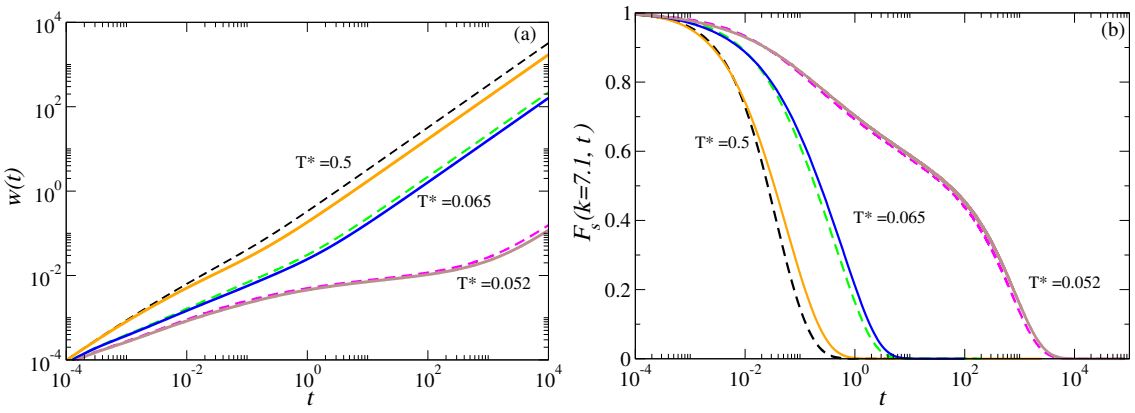

FIG. 8: The mean square displacement and the self-intermediate $F^s(k,t;\phi=0.35)$ as function of temperature $T^*=(1/K)$ with fixed $z=20$ and $\phi=0.35$. The shell thickness $(\sigma_s-\sigma_{in})/2=0.05$ (or $\sigma_{in}=0.9$) and yolk diameter $\sigma_y=0.2$. The solid lines is the theoretical prediction of the SCGLE theory with $\delta=1$. The dashed lines is the theoretical prediction of the SCGLE theory for the empty shell with $D_s^0=1$.

which correspond to the SCGLE theory results for the MSD $W_0(t;T^*=0.5)$ of a liquid of empty shells (or solid attractive hard-spheres) at the same temperature $T^*=0.5$, and which diffuse with the same short-time self-diffusion coefficient D_s^0 as the shells in the yolk-shell system. The yolk-shell repulsive interactions is more important in this temperature than the attraction between shells. The yolk-shell system lead to a MSD $W(t;T^*=0.5)$ that clearly deviates from the empty shell result. Upon decreasing the temperature to $T^*=0.065$ (Fig. 5b), we observe that the deviation of $W(t;T^*=0.065)$ from $W_0(t;T^*=0.065)$ is smaller than the deviation observed at $T^*=0.5$.This means that for this temperature the mutual friction effects due to shell-shell interactions overwhelm the "internal" friction effects due to yolk-shell interactions. If continue decrease the temperature until $T^*=0.052$, we observe that the deviation of $W(t;T^*=0.052)$ from $W_0(t;T^*=0.052)$ is not clear than the previous temperatures. This suggests that the shell-shell attraction is more dominant than the yolk-shell repulsive intereaction.

We next analyze the results for the self-intermediate scattering function of shell-shell $F^s(k,t)$ obtained of our simulation. Let us first discuss the results in figure 8b, where the solid lines are the self-ISF $F^s(k,t;T^*=0.5)$ of yolk-shell particles with dynamic asymmetry $\delta=1$ at a volume fraction $\phi=0.35$. We compare these results with the self-ISF $F_0^s(k,t;T^*=0.5)$ of a liquid of empty-shells at the same volume fraction and with short-time self-diffusion

coefficient $D_s^0 = 1$, plotted as dashed line. We evaluate the self-ISF for three cases at $k = 7.1$, which is approximately the first peak of the $S(k)$. We observe that the relaxation of $F^s(k, t; T^* = 0.5)$ suffers a deviation from $F_0^s(k, t; T^* = 0.5)$, and this is also evidence of the additional friction effect upon the yolk-shell interaction. Upon decrease the temperature to $T^* = 0.065$ and $T^* = 0.052$ (Fig. 8b). We corroborates the observations of the MSD.

D. Effects of yolk-yolk repulsions

With the SCGLE theory above one could still model many other possible physical conditions. The previous illustrative exercise, for example, corresponds to a realistic experiment in which one adds a depletant agent to induce attractions between shells in a yolk-shell suspension with hard-body interactions. One can also imagine, instead, the possibility that the yolks are highly charged colloidal particles encapsulated inside a rigid but electrostatically inert shell, which only hinders its motion. If the screening length is sufficiently large compared with the outer diameter of the shell and with the mean interparticle distance $d = n^{-1/3}$, one can now neglect the shell-shell interactions, since the strong yolk-yolk repulsion will prevent direct contact between shells. Under these conditions, we can notice that the same theory above, with the roles of the yolks and shells interchanged, provides a description of the dynamics of the yolks, renormalized by the averaged effects of the motion of the shells.

In Fig. 9 we illustrate the SCGLE predictions for the self intermediate scattering function of the yolks in a system with no shell-shell interactions, $u_{ss}(r) = 0$, with the same yolk-shell interactions $u_{ys}(r)$ as before (see Eq. (2.8)), and with the yolk-yolk interactions given by

$$\beta u_{yy}(r) = \begin{cases} \infty & \text{for } r < \sigma_y \\ K \frac{exp[-z(r/\sigma_s - 1))]}{r/\sigma_s} & \text{for } r > \sigma_y, \end{cases} \tag{4.6}$$

with $K = 554$ and $z = 0.149$.

V. SUMMARY

In summary, in this paper we systematically studied the dependence of collective diffusion and self-diffusion properties of the yolk-shell complex on the relative mobility (i.e., the ratio ζ_s^0/ζ_y^0), of the shell and yolk particles, and on the concentration of yolk-shell complexes in

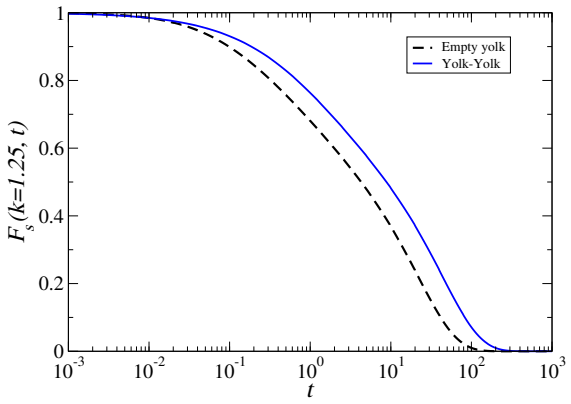

FIG. 9: Self-intermediate scattering function $F^s(k = 1.25, t)$ of the yolks in a system with $u_{ss}(r) = 0$, $u_{ys}(r)$ given by Eq. (2.8), and with the strong yolk-yolk repulsions of Eq. (4.6) with $K = 554$ and $z = 0.149$. The dashed curve corresponds to a free yolk (no shells) with the same repulsive interactions.

the suspension. For this, we assumed purely repulsive hard-body interactions between all (shell and yolk) particles, and carried out systematic Brownian dynamics (BD) simulations to determine the pertinent self- and collective-diffusion properties. In addition, we developed a first-principles theory to predict the main features of the shell-shell dynamic properties (i.e., of $F(k, t)$ and $F_S(k, t)$, etc.) in terms of the specific effective interactions between the shell and the yolk particles that constitute the system. We approached this task in the framework of the self-consistent generalized Langevin equation (SCGLE) theory of colloid dynamics, which was adapted here to the context of a suspension of Brownian yolk-shell particles.

Our results, as obtained from BD and as predicted by SCGLE theory, show that the yolk-shell interaction affects the properties of diffusion of the yolk-shell complex. In the dilute case, our simulations showed that the deviation of the MSD of the yolk-shell complex from the purely diffusive behavior of a empty shell is an indication of the presence of a friction effect upon displacement of the complex due to the yolk-shell interaction. This effect upon the diffusion was more dramatic when we changed the condition of the solvent between the shell and the yolk δ. For example, if the interior of the shell becomes more viscous, so that the ratio δ decreases, then also the diffusivity of the yolk-shell particle will decrease. The predictions of the SCGLE corroborates with the results in the dilute case and follow with good agreement the MSD of our simulations. In the case of the finite concentration, results

describe not only how interactions between yolk and shell influence the dynamic properties of the yolk-shell complex, but also the how they are affected by interactions between the shells. We analyzed the mean square displacement and self-intermediate scattering function of a liquid of yolk-shell particles, and compared them with properties of a liquid of empty shells. We found that at low volume fractions the difference between the dynamic of a yolk-shell complex and the dynamic of an empty-shell, is determined only by the yolk-shell friction, whereas at higher concentrations it is dominated by the shell-shell interactions. Also, our theoretical approach predicted the same scenario obtained for the simulation of the yolk-shell complex as for the empty shell liquid, with a very good agreement.

VI. ACKNOWLEDGMENTS

This work was supported by the U.S. Department of Energy, Office of Basic Energy Sciences, Materials Sciences and Engineering Division. This Research at the SNS at Oak Ridge National Laboratory was sponsored by the Scientific User Facilities Division, Office of Basic Energy Sciences, U.S. Department of Energy.

Appendix A: Averaging over the yolk degrees of freedom.

Let us consider the stochastic but fully microscopic dynamic description of the correlated Brownian motion of the N shell and the corresponding N yolk particles provided by Eqs. (3.1) and (3.2). The purpose of this appendix is to derive in detail from this description the set of N "renormalized" Langevin equations in Eq. (A11), involving the positions and velocities of only the shell particles. If one is interested in observing only the motion of the shell particles, then in principle one needs to solve Eqs. (3.2) for the positions and velocities of the yolk particles, and then substitute in the Eqs. (3.1), averaging over the initial value of the yolks' positions and velocities. This, however, can be done in an alternative manner by re-writing Eq. (3.1) as

$$M_s \frac{d\mathbf{v}_i(t)}{dt} = -\zeta_s^0 \mathbf{v}_i(t) + \mathbf{f}_i^0(t) - \sum_{j\neq i} \nabla_i u_{ss}(|\mathbf{x}_i(t) - \mathbf{x}_j(t)|) + \int d^3\mathbf{r}[\nabla u_{ys}(r)] n_y^*(\mathbf{r}, t). \quad \text{(A1)}$$

where $n_y^*(\mathbf{r}, t)$, defined as $n_y^*(\mathbf{r}, t) \equiv n_y(\mathbf{x}_i(t) + \mathbf{r}, t)$, with $n_y(\mathbf{x}, t) \equiv \delta(\mathbf{x} - \mathbf{y}_i(t))$, is the probability that at time t the center of the yolk particle is located at position $\mathbf{r}$ (referred

to the center of the ith shell particle). This means that the direct pairwise potential $u_{ys}(r)$ between the shell and its yolk couples *exactly* the motion of the shell particle with the motion of its yolk *only* through the variable $n^*(\mathbf{r},t)$.

Since Eq. (3.2) is an ordinary Langevin equation for a Brownian particle in the confining field of the shell, it is equivalent to a Fokker-Planck (FP) equation for the probability $P^*(\mathbf{v},\mathbf{r};t)$ that the yolk has velocity $\mathbf{v}$ and position $\mathbf{r}$ at time t. In the limit of overdamping ($t \gg M^{(y)}/\zeta^{(y)}$), and integrating out the velocity of the yolk, such FP equation becomes the Smoluchowski (or diffusion) equation for a single Brownian particle in the external potential $u^{(ys)}(r)$, which can be written as the following equation for $n_y^*(\mathbf{r},t) = \int d^3v P^*(\mathbf{v},\mathbf{r};t)$

$$\frac{\partial n_y^*(\mathbf{r},t)}{dt} = [\nabla n_y^*(\mathbf{r},t)]\cdot\mathbf{v}_T(t) + D_y^0\nabla^2 n_y^*(\mathbf{r},t) + D_y^0\nabla\cdot n_y^*(\mathbf{r},t)\nabla\beta u_{ys}(r), \qquad \text{(A2)}$$

where the first term on the *r.h.s.* is a streaming term (due to the fact that $n_y^*(\mathbf{r},t) \equiv n_y(\mathbf{x}_T(t)+\mathbf{r},t)$) and $D_y^0 \equiv k_BT/\zeta_y^0$ is the diffusion coefficient of the yolk particle inside the shell tracer particle.

Eqs. (A1) and (A2) are two coupled equations for the variables $\mathbf{v}_T(t)$ and $n_y^*(\mathbf{r},t)$, which involve the non-linear streaming term $[\nabla n_y^*(\mathbf{r},t)]\cdot\mathbf{v}_T(t)$. What we need, however, is the stochastic and linearized version (around the equilibrium values $\mathbf{v}_T^{eq}=0$ and $n_y^{eq}(r)$) of Eqs. (A1) and (A2). For this, notice that $n_y^{eq}(r)$, is given by

$$n_y^{eq}(r) = \frac{e^{-\beta u_{ys}(r)}}{\int e^{-\beta u_{ys}(r)}d^3r}, \qquad \text{(A3)}$$

and that, due to the radial symmetry of the force $[-\nabla u_{ys}(r)]$ and of $n_y^{eq}(r)$, the second integral in Eq. (A1), evaluated at $n_y^*(\mathbf{r},t) = n_y^{eq}(r)$, vanishes. The resulting fluctuating linearized version of Eqs. (A1) and (A2) can thus be written as

$$M_s\frac{d\mathbf{v}_i(t)}{dt} = -\zeta_s^0\mathbf{v}_i(t) + \mathbf{f}_i^0(t) - \sum_{j\neq i}\nabla_i u_{ss}(|\mathbf{x}_i(t)-\mathbf{x}_j(t)|) + \int d^3\mathbf{r}[\nabla u_{ys}(r)]\delta n_y^*(\mathbf{r},t), \quad \text{(A4)}$$

with $\delta n_y^*(\mathbf{r},t) \equiv n_y^*(\mathbf{r},t) - n_y^{eq}(r)$, and

$$\frac{\partial \delta n_y^*(\mathbf{r},t)}{dt} = [\nabla n_y^{eq}(r)]\cdot\mathbf{v}_T(t) + D_y^0\nabla^2\delta n_y^*(\mathbf{r},t) + D_y^0\nabla\cdot\delta n_y^*(\mathbf{r},t)\nabla\beta u_{ys}(r) + f_y^0(\mathbf{r},t), \quad \text{(A5)}$$

where $f_y^0(\mathbf{r},t)$ is a Gaussian fluctuating term with zero mean value and time-correlation function given by the fluctuation-dissipation relation $\langle f_y^0(\mathbf{r},t)f_y^0(\mathbf{r}',t')\rangle = [D_y^0\nabla^2\delta(\mathbf{r}-\mathbf{r}')]n_y^{eq}(r')2\delta(t-t')$.

Formally solving Eq. (A5) and substituting the solution for $\delta n_y^*(\mathbf{r},t)$ in Eq. (A4), leads to

$$M_s\frac{d\mathbf{v}_i(t)}{dt} = -\zeta_s^0\mathbf{v}_i(t) - \int_0^t dt'\ \overset{\leftrightarrow}{\Delta\zeta_y}(t-t')\cdot\mathbf{v}_i(t') + \mathbf{F}_i(t) - \sum_{j\neq i}\nabla_i u_{ss}(|\mathbf{x}_i(t)-\mathbf{x}_j(t)|), \quad \text{(A6)}$$

where the new fluctuating force $\mathbf{F}_i(t)$ has zero mean and correlation function given by the fluctuation-dissipation relation $\langle\mathbf{F}_i(t)\mathbf{F}_j(0)\rangle = k_BT[\zeta_s^0 2\delta(t) + \Delta\zeta_y(t)]\delta_{ij}\ \overset{\leftrightarrow}{\mathbf{I}}$ (with $i,j = 1,2,\ldots,N$) and with the time-dependent friction function $\overset{\leftrightarrow}{\Delta\zeta_y}(t)$ given by the following *exact* result:

$$\Delta\overset{\leftrightarrow}{\zeta}_y(t) = -\int d^3r\int d^3r'[\nabla u_{ys}(r)]\chi_y^*(\mathbf{r}-\mathbf{r}';t)[\nabla' n_y^{eq}(r')]. \quad \text{(A7)}$$

In this equation, $\chi_y^*(\mathbf{r}-\mathbf{r}';t)$ is the Green's function of the diffusion equation in Eq. (A5), i.e., it is the solution of

$$\frac{\partial\chi_y^*(\mathbf{r}-\mathbf{r}';t)}{dt} = D_y^0\nabla^2\chi_y^*(\mathbf{r}-\mathbf{r}';t) + D_y^0\nabla\cdot\chi_y^*(\mathbf{r}-\mathbf{r}';t)\nabla\beta u_{ys}(r) \quad \text{(A8)}$$

with initial condition $\chi_y^*(\mathbf{r}-\mathbf{r}';0) = \delta(\mathbf{r}-\mathbf{r}')$.

Using the fact that $\nabla n_y^{eq}(r) = -\beta n_y^{eq}(r)\nabla u_{ys}(r)$, the previous expression for $\Delta\overset{\leftrightarrow}{\zeta}_y(t)$ can also be written as

$$\Delta\overset{\leftrightarrow}{\zeta}_y(t) = k_BT\int d^3r\int d^3r'[\nabla n_y^{eq}(r)]\left\{\frac{\chi_y^*(\mathbf{r}-\mathbf{r}';t)}{n_y^{eq}(r)}\right\}[\nabla' n_y^{eq}(r')]. \quad \text{(A9)}$$

This expression can be further simplified by introducing the homogeneity approximation, which consists of approximating $[\chi_y^*(\mathbf{r}-\mathbf{r}';t)/n_y^{eq}(r)]$ by $[\chi_y^*(|\ \mathbf{r}-\mathbf{r}'\ |;t)/n_0]$ in the integrand, which allows us to introduce the Fourier transform (FT) $\chi_y^*(k;t)$ of $\chi_y^*(r;t)$, with the result

$$\Delta\overset{\leftrightarrow}{\zeta}_y(t) = \frac{k_BTn_0}{(2\pi)^3}\int d^3k\mathbf{kk}[g_y(k)]^2\chi_y^*(k;t)\ . \quad \text{(A10)}$$

At this point we introduce the so-called decoupling approximation, explained in Ref. [24], which approximates $\chi_y^*(k;t)$ by the product $\chi_y(k;t)F_S(k,t)$, in which $F_S(k,t)$ is the shell intermediate scattering function and $\chi_y(k;t)$ (without the asterisk indicating the moving reference frame of the shell), which can be approximated by the Gaussian approximation with a simple short-time expression for the mean squared displacement $W_y(t)$ of the yolk, namely, $\chi_y(k;t)\approx\exp[-k^2D_y^0t]$. Using these approximations, and taking into account that

the tensor $\Delta \overleftrightarrow{\zeta}_y(t)$ must be isotropic, so that it can be written as $\Delta \overleftrightarrow{\zeta}_y(t) = \Delta\zeta_y(t) \overleftrightarrow{\mathbf{I}}$, we may rewrite the yolk-averaged N-particle Langevin equation in Eq. (A6) as

$$M_s \frac{d\mathbf{v}_i(t)}{dt} = -\zeta_s^0 \mathbf{v}_i(t) - \int_0^t dt' \Delta\zeta_y(t-t')\mathbf{v}_i(t') + \mathbf{F}_i(t) - \sum_{j\neq i} \nabla_i u_{ss}(|\mathbf{x}_i(t) - \mathbf{x}_j(t)|) \quad \text{(A11)}$$

with the scalar time-dependent friction function $\Delta\zeta_y(t)$ given by one third of the trace of $\Delta \overleftrightarrow{\zeta}_Y(t)$, i.e., by

$$\Delta\zeta_y(t) = \frac{k_B T n_0}{3(2\pi)^3} \int d^3k [k g_y(k)]^2 e^{-k^2 D_y^0 t} F_S(k,t). \quad \text{(A12)}$$

---

[1] X.W. Lou, L. A. Archer, Z. Yang, Adv. Mater. 2008, **20**, 3987.

[2] K. Kamata, Y. Lu, Y. N. Xia, J. Am. Chem. Soc. 2003, **125**, 2384.

[3] J. Liu, H. Xia, D. F. Xue, L. Lu, J. Am. Chem. Soc. 2009, **131**, 12086.

[4] H. X. Li, Z. F. Bian, J. Zhu, Y. N. Huo, H. X. Li, Y. F. Lu, J. Am. Chem. Soc. 2007, **129**, 8406.

[5] A. Okada, D. Nagao, T. Ueno, H. Ishii, and M. Konno, Langmuir **29**, 9004 (2013).

[6] P. N. Pusey in *Liquids, Freezing and Glass Transition*, edited by J. P. Hansen, D. Levesque, and J. Zinn-Justin (Elsevier, Amsterdam, 1991), Chap. 10.

[7] J. Brader, J. Phys.: Condens. Matter, **22**, 363101 (2010).

[8] M. Medina-Noyola, Phys. Rev. Lett. **60**, 2705 (1988).

[9] J. F. Brady, Journal of Fluid Mechanics 272, 109 (2006)

[10] A. E. Cervantes-Martínez, A. Ramírez-Saito, R. Armenta-Calderón, M. A. Ojeda-López, and J. L. Arauz-Lara, Phys. Rev. E **83**, 030402(R) (2011)

[11] D. L. Ermak and J. A. McCammon. J. Chem. Phys. **69**, 1352 (1978).

[12] Allen, M. P.; Tildesley, D. J. Computer Simulation of Liquids. Oxford University Press: Oxford, 1989.

[13] F. de J. Guevara-Rodríguez and M.Medina-Noyola, Phys. Rev. E **68**, 011405 (2003).

[14] L. Lopez-Flores, et al.,Phys. Rev. E **88**, 042301 (2013)

[15] J. K. Percus and G. J. Yevick, Phys. Rev. **110**, 1 (1957).

[16] L. Verlet and J.-J. Weis, Phys. Rev. A **5** 939 (1972).

[17] D. Dubbeldam, D. C. Ford, D. E. Ellis, and R. Q. Snurr, Mol. Sim. **35**, 1084 (2009).

[18] L. Yeomans-Reyna and M. Medina-Noyola, Phys. Rev. E **62**, 3382 (2000).

[19] L. Yeomans-Reyna and M. Medina-Noyola, Phys. Rev. E **64**, 066114 (2001).

[20] L. Yeomans-Reyna, H. Acuña-Campa, F. Guevara-Rodríguez, and M. Medina-Noyola, Phys. Rev. E **67**, 021108 (2003).

[21] P.E. Ramírez-González *et al.*, Rev. Mex. Física **53**, 327 (2007).

[22] L. Yeomans-Reyna *et al.*, Phys. Rev. E **76**, 041504 (2007).

[23] R. Juárez-Maldonado *et al.*, Phys. Rev. E **76**, 062502 (2007).

[24] M. Medina-Noyola, Faraday Discuss. Chem. Soc. **83**, 21 (1987).

[25] L. López-Flores, L. L. Yeomans-Reyna and M. Medina-Noyola, J. Phys.: Condens. Matter **24**, 375107 (2012).

[26] .E. Ramírez-González *et al.*, S. Vizcarra-Rendon, F. Guevara-Rodríguez and M. Medina-Noyola, J.Phys. Condens.: Matter **20**, 205104 (2008).

[27] Bergenholtz J. and Fuchs M, Phys. Rev. E, **20** 5706 (1999)

[28] Hoye. J. S and Blum. L , J. Stat. Phys. **16**, 399, (1977)